Finite size effects during the penetration of objects in a granular medium

Valentin Paume, Pascale Aussillous, Olivier Pouliquen

Soft Matter

ARTICLE TYPE

Cite this: DOI: 00.0000/xxxxxxxxxx

Finite size effects during the penetration of objects in a granular medium†

Valentin Paume*[a], Pascale Aussillous[a] and Olivier Pouliquen[a]

Received Date
Accepted Date

DOI: 00.0000/xxxxxxxxxx

In many industrial or geotechnical applications, objects move through a granular medium and an important issue is the prediction of the force that develops during the motion of the intruder. In this paper, we experimentally study the vertical penetration of intruders into granular media and analyze both the average force and the fluctuations during motion. We investigate configurations where the size of the intruder becomes close to a few grain sizes, a regime that has not been studied before. Finite size effects are observed, showing that both the mean force and the fluctuations significantly increase when decreasing the ratio of the intruder size to the particle size, and scaling laws are identified to characterize this effect. The role of a conical tip in front of the cylinder to facilitate the penetration is also studied, showing that it is more efficient when the aspect ratio between the intruder size and the grain size is low.

1 Introduction

The study of the force experienced by an object moving in a fluid represents an entire branch of fluid mechanics. While most studies focus on Newtonian fluids, research on the motion of objects in soft materials such as polymers[1,2], foams[3,4], mud[5,6] or sand[7] is gaining more and more interest, showing that the rheological properties of the medium have a strong and non-trivial influence on the force experienced by the objects. This is particularly true in the case of granular media, which are the focus of the present study, devoted to the penetration of a cylinder in a packing of grains.

The problem of the force generated by an object moving in a granular medium is a central issue in many industrial applications (mixing, mining applications, soil testing in geotechnics, locomotion of animals and robots on sand[8–10], anchoring strategies[11]..). From a fundamental point of view, different configurations have been studied: objects pulled horizontally in a granular material[12,13], plates or cylinders rotating in the medium[14,15], intruders penetrating vertically in the grains[16–19], objects impacting the granular packing[20,21]... In all these situations the forces are controlled to first order by the frictional nature of the rheology of granular materials[22], in which the shear stresses are proportional to the compressive stress[23]. As in all the above configurations the packing lies under gravity, the compressive stress is controlled by the hydrostatic pressure, and one therefore expects that the depth at which the intruder moves in the material plays a fundamental role in the resistance force to movement.

This explains the first important result observed in previous studies, showing that the resistive force on an object moving slowly in a granular material is proportional to the depth at which it is moving multiplied by the cross section of the object. In the case of a fully immersed intruder moving horizontally at depth z, the force thus increases linearly with z. When the intruder is partially immersed (typically a vertical cylindrical plow pulled horizontally), the cross section being itself proportional to the depth, the force varies with the square of the depth z. As the velocity of the motion increases, inertial effects eventually becomes important and a velocity-dependence is observed[24], a situation typically encountered in impact problems[21]. Other parameters like the preparation of the packing[25] or the number of cycling of the motion also modify the penetration forces[26].

A second non-trivial important result is the existence of a lift force on an object moving horizontally in grains, even if the object is symmetrical, an effect explained by the presence of the gravity-induced pressure gradient, which breaks the top/bottom symmetry[27,28]. More generally, the shape of the object and the direction of its motion relative to gravity influence the total force experienced by the object. An attempt to predict the force for arbitrary shaped objects has been proposed in the framework of a resistance force theory (RFT)[29–31]. In this approach, the surface of the object is divided into elementary surfaces, and the total force is assumed to be the sum of the forces that the surfaces would experienced if there were alone in the same position with the same inclination. This approach provides good predictions when the object is moving near the free surface.

In this paper we focus on the configuration of a cylinder pen-

[a]Aix-Marseille Université, CNRS, IUSTI, Marseille, France.
*valentin.paume@univ-amu.fr

etrating vertically a granular material, a system reminiscent of the penetration test in geotechnics and extensively studied in the literature[32,33]. Cone penetration test (CPT) consists in pushing a cylinder with a conical tip in the soil, and in monitoring the forces experiences both by the cone and the cylinder during penetration. The evolution of the forces along the depth provides information about the structure of the soil and the composition of the different layers. Considering the model configuration of a cylinder penetrating a cohesionless granular material, the penetration force F is known to be proportional to cylinder cross-section S times the depth of penetration z: $F = K_n \rho_p g z S$, where ρ_p is the particle density and g the gravity intensity[17,34]. The dimensionless coefficient K_n depends on the properties of the granular material. Assuming that the granular material behaves like a Mohr-Coulomb plastic material, K_n can be computed[17,35] and is found to be a function of the friction coefficient μ of the material, increasing exponentially with μ. Experimental measurement of the penetration force in different materials with different friction coefficients are well predicted by this theory in the limit of large intruders compared to the grain size[17].

Our goal in this study is to examine how the penetrating force deviates from this prediction as the intruder size approaches the grain size, a situation encountered in many applications. In this regime where granular flows occur on sizes less than 10 particle diameters, finite size effects are known to play a major role as observed in shear bands, in flows of thin layers[36], in flows around small objects[28]... These finite size effects are a subject of an active research and have been attributed to the presence of non local effects, which are described by more elaborate constitutive laws than the simple Mohr Coulomb or $\mu(I)$ rheology[37–39]. The existence of finite size effects during penetration of object has been observed in experimental studies[18,40] and has been investigated by Miyai *et al.*[19] using quasi-2D simulations. The authors reported that the penetration force increases with particle size and correlated this variation with the change in the width of the shear bands created during motion. In this paper, we experimentally investigate how finite size effects influence the average penetration force of an object penetrating a 3D granular material, but also how they strongly affect the force fluctuations. We also analyse the role of a conical tip at the head of the cylinder in facilitating the penetration[41].

The setup and experimental procedure are presented in Section 2. In Section 3, we show that finite size effects play a major role in significantly increasing not only the average penetration force, but also the fluctuations that are enhanced as the size of the intruder approaches that of the particle. In Section 4, we investigate how sharpening the cylinder tip may facilitate penetration, especially in the regime of finite size effects. Section 5 presents conclusions and perspectives.

2 Experimental Method

The experimental setup is shown in Fig. 1. A cylindrical container of diameter $D_c = 200$ mm is filled with particles to a height $H = 130$ mm. An intruder is moved vertically through the granular material by a vertical linear actuator (ZEMA, Zwick Roell). A force sensor placed between the actuator and the intruder provides an accurate measurement of the penetration force during the movement. We used two different sensors with a nominal force of 10N and 100N (accuracy of 0.5%) and we record the data at a frequency of 50Hz. The intruders are 3D printed in PLA with a 0.4 mm nozzle and a layer thickness of 0.1 mm. We checked that the results are quantitatively identical using smooth metal intruder of the same shape, showing that the tiny roughness induced by the layering inherent to 3D printing does not play a role in the regime investigated in this study.

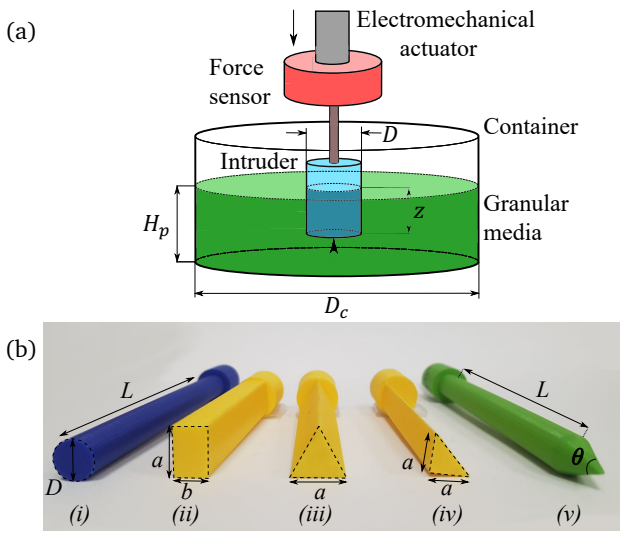

Fig. 1 a) Sketch of the experimental setup consisting in a linear motor connected to the intruder by a force sensor. b) Picture of the different intruders used in the study: *(i)* cylinders (various D, $L = 110$mm), *(ii)* rectangular section ($a \times b = 10 \times 10$, 12.5×8, 20×5 mm^2 and $L = 70$ mm), *(iii)* equilateral triangle section ($a = 13$ mm and $L = 70$ mm), *(iv)* rectangular triangle section ($a = 9.5$ mm and $L = 70$ mm), *(v)* conical shape (various θ, $D = 10$mm and $L = 110$mm).

The intruders used are mainly cylindrical with a length $L = 110$ mm and different diameters $D = 3, 5, 10, 15, 20, 30, 40, 50$ mm. Other shapes are also tested with different cross sections as shown in Fig. 1b (rectangular and triangular cross section). For these shapes, an equivalent diameter D is defined as $D = \sqrt{4S_n/\pi}$, where S_n is the intruder cross section area. The influence of the presence of a conical tip is also studied for $D = 10$ mm, by varying the tip angle θ in the range $20, 60, 80, 100$ and 120 deg. All the experiments are performed in the limit of a large container, whose diameter D_c is large compared to the intruder size and to penetration depth, to ensure that the container walls do not influence the results and that there is no Janssen effect .

The granular media are made of monodisperse spherical glass beads of density $\rho_p = 2500$ kg.m^{-3} with different mean diameters $d_p = 0.135, 0.52, 1.2, 3.0$ and 4.5 mm, supplied by SiLiBeads (Deco Beads) and by Bellco (for $d_p = 3.0$mm).

Prior to the intruder penetration, the granular packing is prepared as follows. The grains are stirred with a spatula. Then the container is slightly shaken horizontally to obtain a flat surface. After this preparation, we expect the granular medium to be in a critical state, with the initial volume fraction estimated to be around 0.58. The intruder initially above the granular free sur-

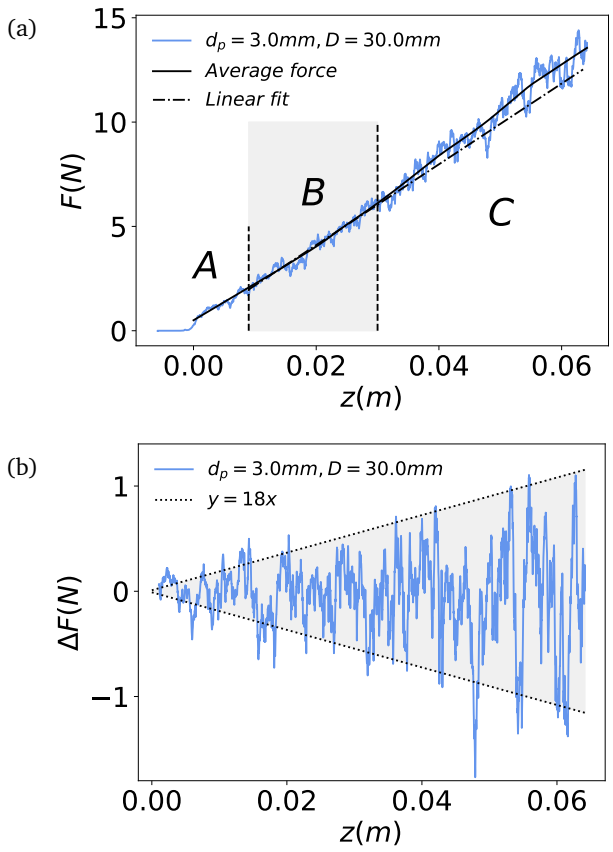

Fig. 2 a) Vertical force measurement F versus the penetration depth z for a cylindrical intruder $D = 30$ mm penetrating a granular media $d_p = 3$ mm. The solid line represents the average force $\langle F \rangle$ computed with the LOWESS method and the dash-dotted line the linear fit in the B region. b) Force fluctuation $\Delta F = F - \langle F \rangle$ as a function of z (lines are guide for the eyes showing the linear increase of ΔF with z).

face is then moved vertically downward at a slow and constant speed $v = 0.5$ mm/s to ensure that the entire penetration process remains in a quasi-static regime[7]. During penetration, the vertical displacement and the vertical drag force are recorded. Each experiment is repeated 4 to 10 times.

Fig. 2a shows the evolution of the raw force as a function of the penetration depth z, for a cylindrical intruder $D = 30$ mm in a granular medium $d_p = 3$mm. We define the position of the granular medium surface, $z = 0$, when the vertical force reaches the threshold value $F = max(0.5\rho_p g S D, 10$ mN$)$. As expected, we observe that the force increases almost linearly with the penetration depth. The signal also shows that fluctuations are present around the average increase of the force. To analyse the signal, we decompose the raw force into an average and a fluctuating part $F(z) = \langle F \rangle(z) + \Delta F(z)$. The smoothed average force is computed using the LOcally WEighted Scatterplot Smoothing (LOWESS) algorithm[42], based on a weighted local averaging over a spatial window λ_{av}. In the following, the smoothing window is chosen equal to $\lambda_{av} = 6d_p$, motivated by the observation discussed later in the paper that the typical period of the fluctuation is proportional to the particle diameter ($\approx 3d_p$). The smoothed force $\langle F \rangle(z)$ resulting from this average procedure is plotted as a solid line in Fig.2a and the fluctuating part $\Delta F(z)$ is plotted in Fig.2b as a function of displacement. In the next section, we analyse how the average force and the fluctuations vary with the experimental parameters for flat bottomed intruders, with a focus on the role of the aspect ratio between the intruder size and the grain size.

3 Penetration of flat-bottomed intruders

In this section we focus on the case of flat-bottomed intruders shown in Fig. 1 (*i-iv*). To characterise the evolution of the force during penetration, we consider a classical description developed in previous approaches[18,19], based on the assumption that the material behaves as a frictional plastic material. The resistance force is written as a sum of two contributions related respectively to the tip and to the side walls. The first contribution F_n is due to the normal stress that applies to the front flat surface of the intruder as it pushes the granular material in front of it. It is proportional to the local pressure in the medium and can be written as $F_n = K_n \rho_p g z S_n$, where K_n is a dimensionless constant, ρ_p the density of the grains, z the penetration depth and $S_n = \pi D^2/4$ the cross-section of the intruder. In the framework of a Mohr-Colomb material, K_n can be computed as a function of the friction coefficient μ of the granular material[17,35]. The second contribution is due to tangential stress induced by the friction of the grains sliding on the side walls of the intruder and can be written as $F_t = K_t \int_0^z \rho_p g \pi D z' dz' = K_t \rho_p g \pi D z^2/2$, where K_t is a dimensionless constant equal to the wall/grains friction coefficient. Defining the dimensionless force $\tilde{F} = 4F/\rho_p g \pi D^3$ based on an Archimedes scaling and the dimensionless penetration depth $\tilde{z} = z/D$, the force can then be expressed as follows:

$$\langle \tilde{F} \rangle = c_0 + K_n \tilde{z} + 2K_t \tilde{z}^2. \quad (1)$$

The constant c_0 comes from the fact that just at the beginning of the penetration a small force jump is observed that corresponds to the mobilisation of a stagnant zone in front of the object[16–18]. The example shown in Fig. 2a illustrates the relevance of this description, showing the tiny initial jump (region A), the linear regime (region B) and the slight non linearity observed at high depth (region C). From the smoothed force data (the solid line in Fig.2a), we can obtain the coefficient K_n using a linear fit on the interval $\tilde{z}^{fit} = [0.3; 1]$. The lower limit takes into account the initial non-linear regime. The upper limit insures that the fitting region is large enough, while remaining in the linear regime. Once K_n is determined, we also measure the coefficient K_t of the nonlinear term by a quadratic fit on the whole curve.

Fig. 3 shows for two different granular media of increasing size d_p, how the dimensionless force $\tilde{F}$ varies as a function of the dimensionless penetration depth $\tilde{z}$ for different cylindrical intruder diameters D. The first observation is that for the case of the finest grains Fig. 3a, all curves obtained for different intruder sizes collapse indicating that the scaling chosen for the non-dimensionalized force correctly captures the influence of the intruder size. However, the collapse becomes less accurate when increasing the grain size (Figs. 3b). In coarse grains, we observe that both the smoothed average force (solid lines) and the fluctuations seem to increase when decreasing the intruder diameter.

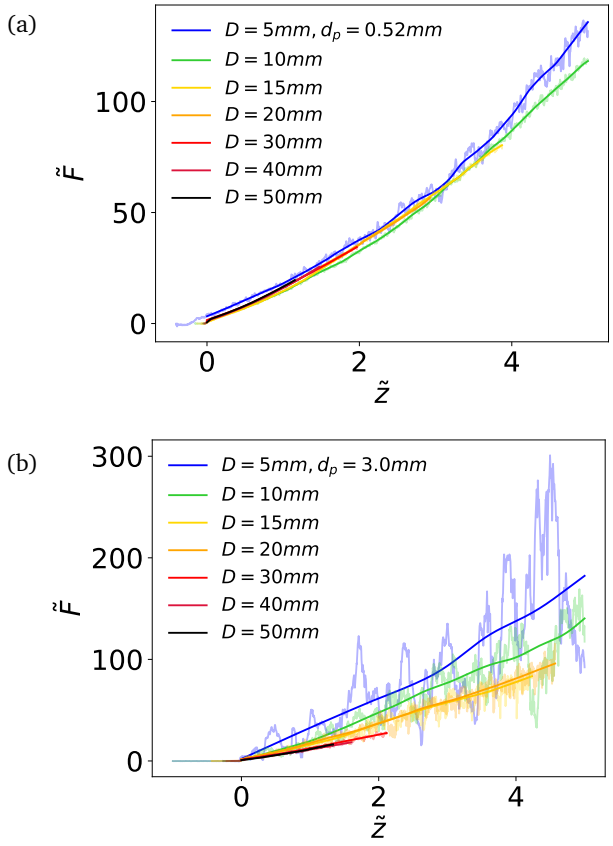

Fig. 3 Dimensionless force $\tilde{F}$ as a function of the penetration depth $\tilde{z}$ for cylindrical intruders of various diameters D in granular material of size a) $d_p = 0.52$ mm and b) $d_p = 3$ mm.

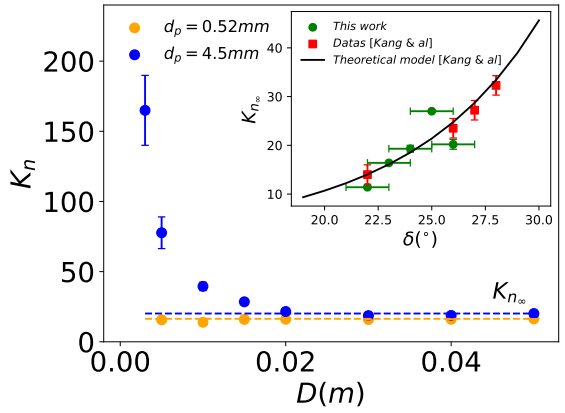

Fig. 4 Evolution of the coefficient K_n as a function of the cylinder diameter D for two different particle sizes d_p. The dashed lines represent the coefficient K_{n_∞} in the limit of large aspect ratio D/d_p. Inset: Evolution of the coefficient K_{n_∞} as a function of the friction angle δ for experimental data from this study and the work of Kang *et al.* [17], compared with the theoretical model of Kang *et al.* [17].

Table 1 Properties of the granular media used in the experiments and the measured K_{n_∞} coefficient.

d_p (mm)	Friction angle δ (°)	*measured* K_{n_∞}
0.135 ± 0.03	25 ± 1	27
0.52 ± 0.10	23 ± 1	16.3
1.20 ± 0.07	24 ± 1	19.3
3.0	22 ± 1	11.4
4.5	26 ± 1	20.2

3.1 Size effect on the smoothed average force

From the evolution of the smoothed force, we compute for each particle size and intruder diameter the coefficient K_n. Figure 4 shows how K_n varies with the intruder diameter for a fine and a coarse granular medium. We observe that for the fine particles ($d_p = 0.52$mm) the coefficient K_n is constant and does not depend on the intruder size D as found by Kang *et al.* [17]. However, for larger particles ($d_p = 4.5$mm), the coefficient K_n increases significantly when decreasing the intruder size [19]. This suggests that in this regime, when the intruder size is close to the grain size, finite size effects are present, where the discrete nature of the granular medium is no longer negligible.

This behavior disappears when $D \gg d_p$, and the coefficient K_n tends towards a constant that we note K_{n_∞}, which we measure for each granular medium. We also measure for each medium the friction angle δ using a rotating drum, which values are reported in table 1. In the inset of figure 4 we compare our measurements of K_{n_∞} with those obtained by Kang *et al.* [17] and with the theoretical model they developed in the continuum framework of the Mohr-Coulomb criterion, predicting the variation of K_n with the angle of friction δ. We observe a good agreement between the experimental values of K_{n_∞} and the model, showing that the Mohr Colomb description is relevant to predict K_{n_∞} when the aspect ratio between the intruder and the grains is large.

To characterise the finite-size effects observed when D/d_p decreases, we plot in Fig. 5a the ratio K_n/K_{n_∞} as a function of the aspect ratio D/d_p for all experiments performed. We observe that all data collapse in this representation, suggesting that the relative increase in the coefficient K_n is controlled by the size ratio between the diameter of the intruder and the particle diameter. The transition between the finite-size regime to the continuum regime occurs for $D \approx 4.5 d_p$. We also reported in Fig. 5a data for other shapes (triangular and rectangular), showing that the shape of the intruder does not play a role. This was observed by Kang *et al.* [17] in the high aspect ratio limit, and we show here that it is also true in the finite size regime.

To explain the role of the particle size, a simple model has been proposed by [14,19], who write that the intruder has an effectif diameter equal to $D + d_p$. The force should then be equal to $F_n = K_{n_\infty} \rho_p g z (D + d_p)^2 \pi/4$, which according to our definition of K_n is also equal to $F_n = K_n \rho_p g z D^2 \pi/4$. This leads to the following prediction

$$K_n/K_{n_\infty} = (1 + d_p/D)^2 \quad (2)$$

The dashed line in Fig. 5a shows that this prediction surprisingly captures the trend of the experimental data, although it predicts a smoother transition between the finite size effects and the continuous regime observed in the experiments.

We also measure the coefficient K_t characterising the departure from linear Archimedes' law due to the frictional interaction on the sides of the intruder. The coefficient K_t is measured in all

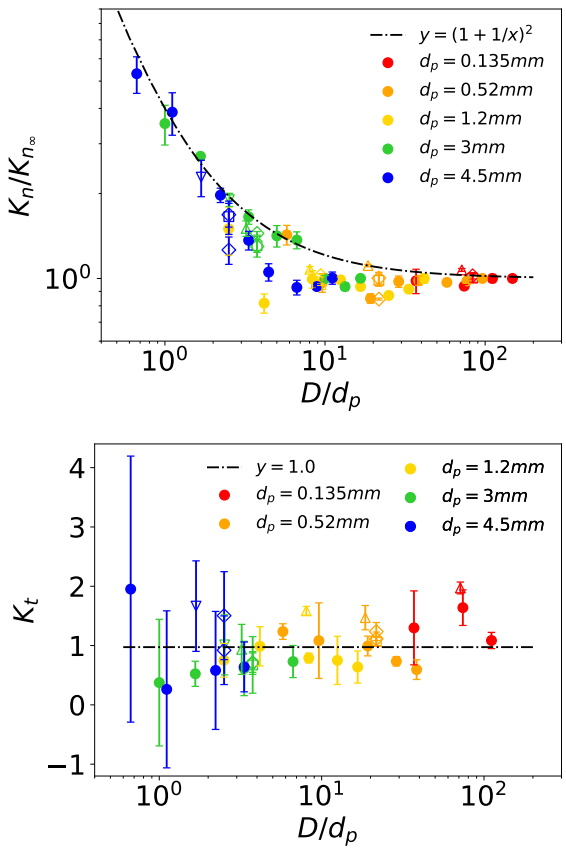

Fig. 5 a) Evolution of the normalised coefficient K_n/K_{n_∞} versus the ratio D/d_p. The dot-dashed line corresponds to eq. 2. b) K_t versus the ratio D/d_p. The dot-dashed line corresponds to the best fit by a constant $K_t = 1.0$. The symbols correspond to the different intruders cross section: circular (•), square (□), rectangles (⋄), equilateral triangle (△), rectangular triangle (▽).

experiments, and Fig. 5b shows how it varies with the aspect ratio D/d_p. Due to the fitting procedure, the data are more noisy for K_t than for K_n, but no systematic influence of the aspect ratio D/d_p is observed, and the coefficient can be considered as constant with the best fit giving $K_t \approx 1.0$. We can then conclude that no finite size effects is observed for the quadratic term of the force as notice in simulation [19]. This observation is coherent with the fact that K_t is related to the wall/grains friction, which for smooth surfaces as used for our intruders is expected to be roughly independent of the grain size, although the value 1 is higher than expected for a wall friction coefficient. We now turn to the analyse of the fluctuating part of the force, which also appears to be sensitive to the finite size effect as observed in the raw data of Fig. 3.

3.2 Force fluctuations

During penetration, the intruder experiences significant force fluctuations, especially when moving in a coarse media. To characterize them, we systematically measure the fluctuations $\Delta F = F - \langle F \rangle$, which like the mean force are expected to grow linearly with the depth. We then define the dimensionless fluctuations by dividing $\Delta F(z)$ by the mean force experienced by the intruder in the continuous limit of very fine grains equal to $K_{n_\infty}\rho_p g z S_n$. The dimensionless fluctuations then writes :

$$\widetilde{\Delta F}(\tilde{z}) = \frac{\Delta F}{K_{n_\infty}\rho_p g z S_n} = \frac{\tilde{F} - \langle \tilde{F} \rangle}{K_{n_\infty}\tilde{z}} \tag{3}$$

An example of $\widetilde{\Delta F}$ as a function of the dimensionless penetration depth $\tilde{z}$ is plotted in the inset of Fig. 6a. The dimensionless signal fluctuates around zero with an amplitude that is constant during the penetration, meaning that ΔF grows linearly with the depth as anticipated by the nondimensionlization of eq. 3. The same feature is observed in all our experiments. We first analyze the spatial period of the fluctuations, by applying a FFT transform to the signal. The average spectrum obtained for $D = 10$mm and different d_p are plotted in Fig. 6b as a function of the wavelength divided by the particle diameter λ/d_p. All the spectrum collapse, with a maximum obtained for $\lambda_{max}/d_p \approx 2.6$. This shows that a well defined periodicity exists in the fluctuations, which is controlled by the grain size d_p and is independent of the intruder size D, as shown inset of Fig. 6b showing that λ_{max}/D varies linearly with d_p/D. This suggest that the fluctuations take their origin in the particle rearrangements at the grains size. This observation justifies a posteriori the choice of an average window $\lambda_{av} = 6d_p \approx 2\lambda_{max}$ to smooth the force curve.

To further characterize the fluctuations, we plot in Fig. 6a a typical distribution of the normalised fluctuations amplitude, showing that they follow a centred normal distribution. From the distribution we extracted the standard deviation $\tilde{\sigma}$ for all our runs, for all grains and intruder sizes. Unlike the period of the fluctuations, the amplitude $\tilde{\sigma}$ varies with the size of the intruder D. The data are plotted in Fig.7 showing how $\tilde{\sigma}$ varies as a function of the aspect ratio D/d_p. All the data obtained in the different granular media, for different sizes and shapes of intruders collapse on a single curve well approximated by a power law. The best fit gives:

$$\tilde{\sigma} = 2\left(\frac{D}{d_p}\right)^{-3/2} \tag{4}$$

In the Appendix A we propose a theoretical explanation for this power law. Based on the assumption that the inter-particle force distribution in a granular material follows an exponential distribution, we show that the scaling given by eq.4 for the force fluctuation simply arises from the statistical average process of the particle forces on a volume of size D^3 in front of the intruder.

In conclusion of our measurements on the flat bottom intruders, we can infer that the ratio of the intruder size to the particle size influences both the average force and the fluctuations. Penetrating a coarse granular media is thus twice penalising if one consider the maximum force necessary to continuously move in the material. In the next section we investigate how a sharper shape may reduce this effect.

4 Influence of a conical tip

The intruder used in this section are cylindrical intruders of diameter $D = 10$mm with a conical tip with zenith angles varying in the range $\theta = 20, 60, 80, 100, 120, 180$ deg, the case $\theta = 180$ deg corresponding to the flat case without conical tip. Figure 8 shows

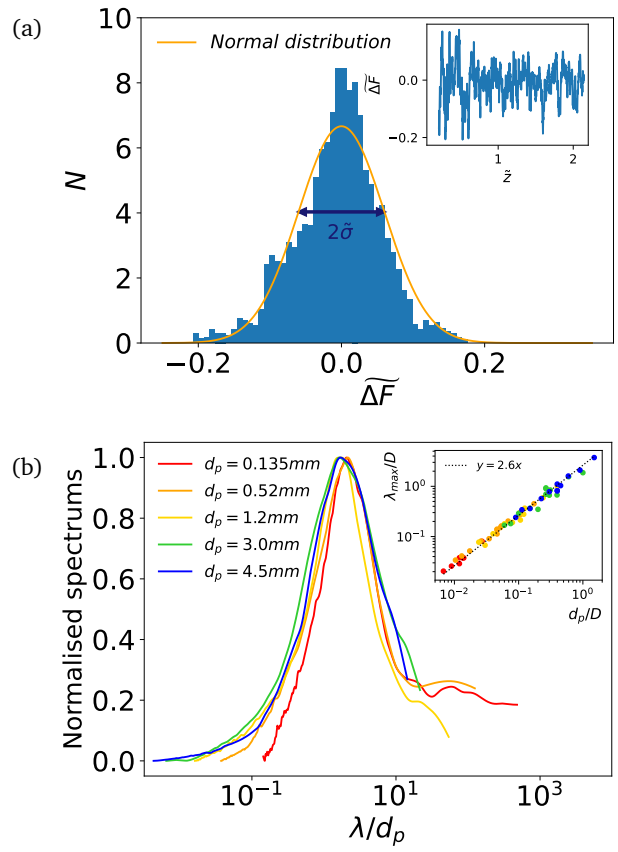

Fig. 6 a) Distribution of the normalised fluctuations $\widetilde{\Delta F}$ for $D = 30$ mm, $d_p = 3$ mm. The orange curve represents a centred normal distribution with a standard deviation $\tilde{\sigma} = 0.06$. Inset : $\widetilde{\Delta F}(\tilde{z})$ for the same data. b) Normalised spectrum versus the wavelength normalised by the particle diameter, λ/d_p, for $D = 10$ mm. Inset: Maximum wavelength λ_{max}/D as a function of d_p/D for different grains and intruders. The dashed line represents $\lambda_{max} = 2.6d_p$.

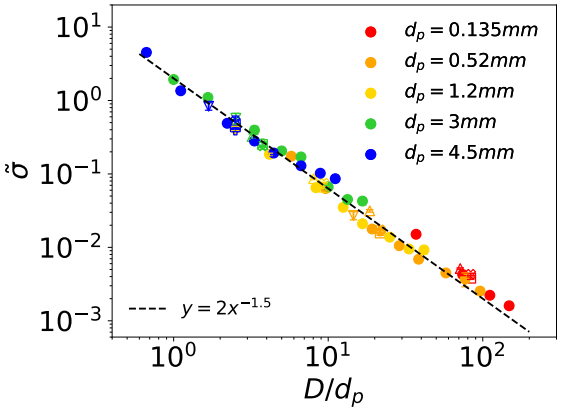

Fig. 7 Amplitude of the force fluctuation $\tilde{\sigma}$ as a function of D/d_p. The dashed line corresponds to eq. 4. The symbols correspond to different intruder cross sections: circular (•), square (□), rectangles (⋄), equilateral triangle (△), rectangular triangle (▽).

the penetration force as a function of the depth for 3 different tip angles ($\theta = 20$, 100 and 180 deg) and for two granular medium $d_p = 0.52$mm and $d_p = 3$mm. The position $z = 0$ is defined when

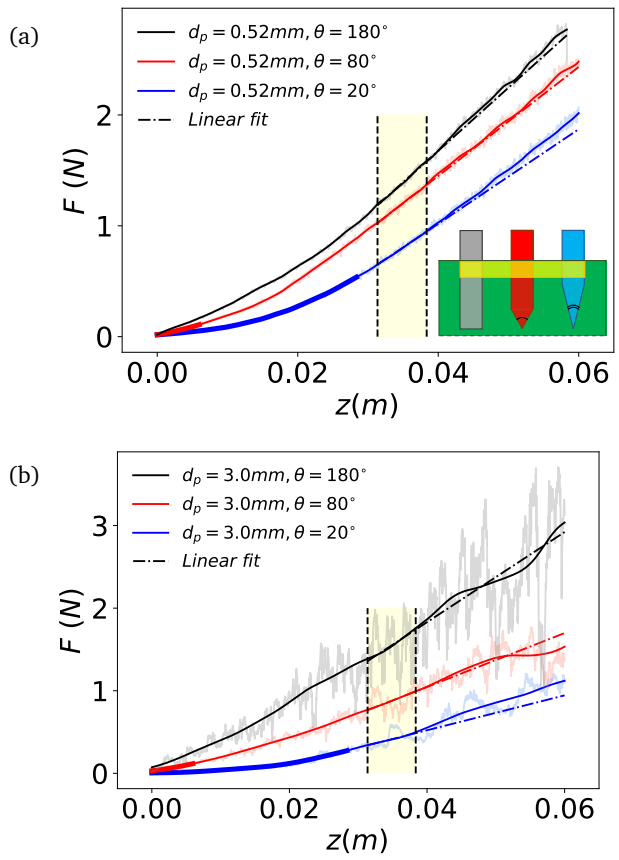

Fig. 8 Force versus the depth of penetration for intruders with conical tips of different zenith angle θ in a granular medium with (a) $d_p = 0.52$mm and (b) $d_p = 3$mm. The continuous lines are the smoothed average force. The bold parts correspond to the penetration of the tip itself. The yellow region corresponds to the interval $[0.3D + h_{tip,20^o}, D + h_{tip,20^o}]$, $h_{tip,20^o}$ being the length of the sharpest cone. The slope in this region (dotted lines) provides a measurement of the parameter K_n^θ, characterizing the difficulty of the cylinder to penetrate behind the tip.

the tip first touches the granular medium. The penetration of the tip initially gives rise to a non linear evolution of the force identified in the figure by the bold part of the curves. This non linearity is due to the increase of the section of the cone during penetration[34]. In order to analyse to which extend the presence of the tip facilitates the subsequent penetration of the cylinder, we analyse the evolution of the force once the tip is fully immersed in the grains at the same penetration depth, i.e in the yellow region in Fig. 8. Two observations can be made. First the force increment necessary to move the cylinder behind the tip seems smaller for sharp tips i.e. small θ compared to flat intruders. Secondly the fluctuations around the mean force seem to be attenuated by the presence of the tip. These two effects are even more pronounced in the case of the penetration in the coarse material (Fig. 8b).

To quantitatively characterize the influence of the tip, we interpolate the smoothed force by a linear function in the yellow region and define the slope $K_n^\theta = d\tilde{F}/d\tilde{z}$, which characterises the difficulty of the cylinder to penetrate behind the tip. Figure 9a shows the evolution of the ratio $K_n^\theta/K_n^{180^o}$ as a function of the tip angle θ for different grain sizes ($\theta = 180^o$ corresponding to the

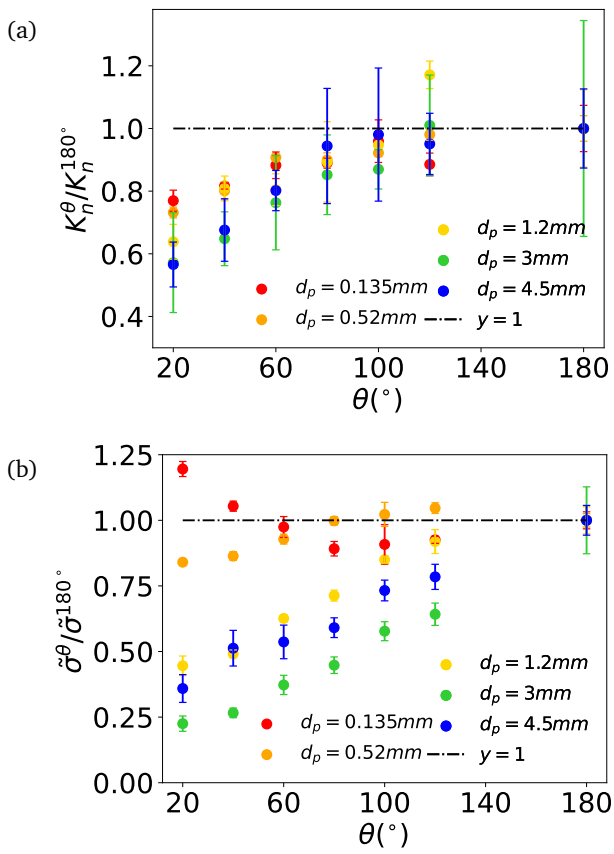

Fig. 9 a) Coefficient $K_n^\theta/K_n^{180^o}$ and b) normalized force fluctuation amplitude $\tilde{\sigma}^\theta/\tilde{\sigma}^{180^o}$ as a function of the tip angle θ for different particle diameters.

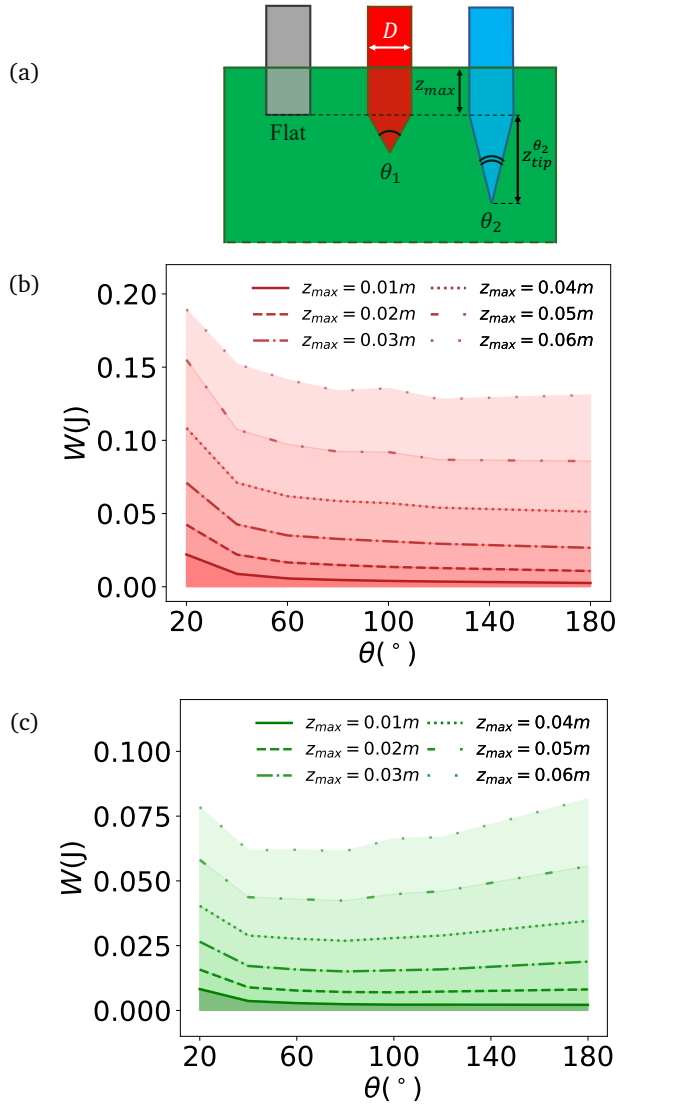

Fig. 10 a) Configurations where the cylinder is inserted a length z_{max} behind the conical tip. b) Work W necessary to reach this configuration as a function of the tip angle for different depth z_{max} in grains of diameter $d_p = 0.135$mm. c) same for $d_p = 3mm$.

flat cylinder). The ratio decreases when decreasing θ below 120^o, meaning that the sharpest the tip, the easiest the penetration of the cylinder behind the tip. The gain is about 40% for the tip with an angle 20% compare to the flat cylinder. This tendency is similar for all the grain size, although it is more pronounced in the coarse grains, meaning that the facilitation by the tip seems more efficient in presence of finite size effects. The observation that tips with an angle less than 120^o do not influence K_n could be linked to the presence of a conical dead zone that exists even with a flat intruder. Adding a conical tip may not change the flow until it is sharper than the natural dead cone.

The presence of the tip also modifies the fluctuations, but only its amplitude and not the period. We have checked that the spectral analysis of the force signal obtained with conical tips reveals the same well defined period given by $\lambda_{max} \approx 3d$. However, the amplitude is significantly affected by the presence of the tip. Fig. 9b shows the standard deviation of the force on intruders with conical tips normalised by the standard deviation for a flat cylinder $\tilde{\sigma}^\theta/\tilde{\sigma}^{180^o}$ as a function of the zenith angle θ for different grains sizes. Different behaviors are observed depending on the grains size. For the finer granular materials $d_p = 0.135$mm and $d_p = 0.52$mm, the standard deviation is more of less independent of the tip angle, with even a small increase observed for the finest grains. However, for coarser grains, a significant decrease of the fluctuation amplitude is observed when decreasing the zenith angle. Fluctuations for $d_p = 4.5$mm are 75% less for the sharp tip $\theta = 20^o$ than for the flat cylinder. The interpretation of the fluctuation attenuation by the tip is not obvious, but might be understood by a geometrical effect: the conical tip pushes the grains on the side when penetrating into the interstices, when the flat cylinder pushes frontally on the grains. This might be less true for the smallest grains, as our 3D printed intruder are rounded at the tip over a typical size of 300μm, which may explain why the attenuation in the force fluctuations in Fig. 9b is not observed for the two smallest grains.

Before concluding this section on the role of a conical tip, we address another question of interest for applications. Is it advantageous to have a conical tip in front of the cylinder if one want to introduce a certain length of the cylinder in the granular medium. In other words, we want to compare the work

necessary to achieve the situations sketched in Fig. 10a, where the same amount of the cylindrical part of the intruder reaches a depth z_{max}. On one hand, adding a tip that has to penetrate first costs some additional work, but on the other hand we know from the above results that the presence of the tip also decreases the force necessary to further move the cylinder behind the tip, meaning that a trade-off might exists. In Figure 10b and c we compute from the experimental measurements the work necessary to achieve different depths z_{max}, and plot it as a function of the tip angle for the finest (Fig. 10b) and the largest grains (fig. 10c) used in our study. Whereas for the fine grains, the minimum work for all depth studied in the experiments is always achieved using a flat cylinder, when penetrating coarse grains an optimum exists : to introduce 6cm of the cylinder in the medium, it is better to use a conical tip with an angle 50^o. This result might explain the use of teeth in some mining applications when working in coarse grains.

5 Conclusion

In this paper, we studied the penetration of cylindrical intruders into a granular medium in a regime where the cylinder size approaches the grain size. We then depart from the continuous limit, and important finite size effects controlled by the aspect ratio between the cylinder size and grains size have been identified.

First of all, the average penetration force increases significantly when the size of the object drops below ten grain sizes, to reach values almost three times greater when the size aspect ratio is one. To account for this increase, the explanation in terms of an increase of the effective cross-section by one grain diameter[14,19] is not totally satisfactory because it predicts a too soft transition, and is based on an oversimplified description of the flow. Another interpretation may be that the observed finite size effects are the signature of a non local rheology. It would then be interesting to test whether recent continuous approaches accounting for finite size effects by non-local terms[37,39] are able to capture the force amplification or not.

We also observed that the ratio of object size to grain size plays a crucial role in the fluctuations of the force. The force signal during penetration exhibits a well defined periodicity corresponding to a length scale equal to about 3 particle diameters and the amplitude of the force fluctuations follows a -3/2 power law with the aspect ratio. The theoretical approach considering that the fluctuations are simply controlled by an averaging process of the inter-particle forces on a volume which scales with the cylinder size provides a good prediction of the scaling law.

From an application perspective, the concomitant growth of the average force and fluctuation as the size of the object decreases (or the size of the grains increases) is crucial in predicting the maximum forces and thus the resistance that the objects will have to undergo during their use. In mining applications, teeth are also often used to dig into coarse granular material. We have analyzed the intuitive idea that a pointed object penetrates more easily a granular material. We have shown that the presence of a conical tip at the head of the cylinder has a quantitative effect on the penetration coefficient K_n, with a decrease varying of about 40% when decreasing the aspect ratio between the object and the grains. The point effect is even more noticeable on the force fluctuations, whose amplitude decreases by nearly 80% when the aspect ratio between the intruder and the grains approaches one. Understanding these intuitive effects is far from trivial. A first step could be the generalization of the plasticity calculation based on a Mohr-Coulomb model to a conical geometry.

FInally, we have restricted our analyse to the case of a single cylinder penetrating a granular medium. However, many applications use systems with several teeth to pick up or mix the grains. The interaction between the objects moving in a granular material is a problem that start to be studied[43–46] and for which finite size effects certainly play an important role.

6 Appendix A: theoretical estimate of the force fluctuations amplitude.

The instantaneous force F experienced by the intruder is equal to $F = P_{zz}D^2$, where P_{zz} is the instantaneous normal stress averaged over the intruder section. P_{zz} can be estimated from the interparticle forces by $P_{zz} = \frac{1}{V}\sum_{c\in V} f_z^c b_z^c$, where f_z^c is the vertical component of the force at contact c, b_z^c the vertical component of the branch vector relating the center of the two particles in contact, and V the representative volume of averaging. The variance of the pressure is then related to the variance of the interparticle force :

$$\mathrm{Var}(P_{zz}) = \frac{n}{V^2}\mathrm{Var}(f_z)d^2 \tag{5}$$

where n is the number of contact c in the volume V. Being interesting on the force that applied at the tip of the intruder of size D, we choose for the representative volume $V \propto D^3$, the volume of the cone in front of the intruder. The number of contact in this volume is then $n \propto (D/d_p)^3$. We also assume that the force distribution follows an exponential distribution as observed in many studies, with an average being related to the average pressure $\langle f_z\rangle \propto \langle P_{zz}\rangle d^2$. This assumption implies that the variance of the force distribution is equal to the square of the mean: $\mathrm{Var}(f_z) = \langle f_z\rangle^2 \propto \langle P_{zz}\rangle^2 d^4$. Equation 6 can then be written as :

$$\frac{\mathrm{Var}(P_{zz})}{\langle P_{zz}\rangle^2} \propto n^{-1} \propto \left(D/d_p\right)^{-3}. \tag{6}$$

This implies that the relative standard deviation of the force $\sqrt{\mathrm{Var}(F)}/\langle F\rangle$ follows a power law : $\sqrt{\mathrm{Var}F}/\langle F\rangle \propto \left(D/d_p\right)^{-3/2}$. One should notice that the dimensionless standard deviation $\tilde{\sigma}$ defined in section 3 is equal to $\tilde{\sigma} = \sqrt{\mathrm{Var}F}/\langle F\rangle \frac{K_n}{K_{n_\infty}}$, and then according to the above argument should not follows strictly the power law as K_n/K_{n_∞} is also a function of D/d_p.

Author Contributions

VP did the experiments measurements. VP, PA and OP contributed to the conception and analysis of the experiments and to the writing of the paper.

Conflicts of interest

There are no conflicts to declare.

Acknowledgements

This work has been funded by Safe Metal. We thank J.-F. Carton, F. Marchand and O. Falcoz for fruitful discussion.

Notes and references

1 J. R. Gladden and A. Belmonte, *Phys. Rev. Lett.*, 2007, **98**, 224501.
2 H. Tabuteau, P. Coussot and J. R. de Bruyn, *Journal of rheology*, 2007, **51**, 125–137.
3 B. Dollet, F. Elias, C. Quilliet, C. Raufaste, M. Aubouy and F. Graner, *Phys. Rev. E*, 2005, **71**, 031403.
4 Z. Jing, S. Wang and Z. Wang, *Langmuir*, 2016, **32**, 2419–2427.
5 N. P. Chafe and J. R. de Bruyn, *J. of Non-newtonian Fluid Mech.*, 2005, **131**, 44–52.
6 P. Coussot, *J. Non-Newtonian Fluid Mech.*, 2014, **211**, 31–49.
7 R. Albert, M. Pfeifer, A.-L. Barabási and P. Schiffer, *Phys. Rev. Lett.*, 1999, **82**, 205.
8 C. Li, T. Zhang and D. I. Goldman, *Science*, 2013, **339**, 1408–1412.
9 R. D. Maladen, Y. Ding, C. Li and D. I. Goldman, *Science*, 2009, **325**, 314–318.
10 N. D. Naclerio, A. Karsai, M. Murray-Cooper, Y. Ozkan-Aydin, E. Aydin, D. I. Goldman and E. W. Hawkes, *Science Robotics*, 2021, **6**, 2922.
11 J. Featherstone, R. Bullard, T. Emm, A. Jackson, R. Reid, S. Shefferman, A. Dove, J. Colwell, J. E. Kollmer and K. E. Daniels, *Planet. Sci. J.*, 2021, **2**, 243.
12 A. Seguin, Y. Bertho, P. Gondret and J. Crassous, *Phys. Rev. Lett.*, 2011, **107**, 048001.
13 M. Kobayakawa, S. Miyai, T. Tsuji and T. Tanaka, *Phys. Rev. E*, 2018, **98**, 052907.
14 R. Soller and S. A. Koehler, *Phys.Rev. E*, 2006, **74**, 021305.
15 F. Guillard, Y. Forterre and O. Pouliquen, *Phys. Rev. Lett.*, 2013, **110**, 138303.
16 T. G. Murthy, E. Gnanamanickam and S. Chandrasekar, *Phys. Rev. E*, 2012, **85**, 061306.
17 W. Kang, Y. Feng, C. Liu and R. Blumenfeld, *Nature Comm.*, 2018, **9**, 1101.
18 Y. Feng, R. Blumenfeld and C. Liu, *Soft matter*, 2019, **15**, 3008–3017.
19 S. Miyai, M. Kobayakawa, T. Tsuji and T. Tanaka, *Granular Matter*, 2019, **21**, 1–21.
20 H. Katsuragi and D. J. Durian, *Nature Physics*, 2007, **3**, 420–423.
21 H. Katsuragi and D. J. Durian, *Phys. Rev. E*, 2013, **87**, 052208.
22 B. Andreotti, Y. Forterre and O. Pouliquen, *Granular media: between fluid and solid*, Cambridge University Press, 2013.
23 P. Jop, Y. Forterre and O. Pouliquen, *Nature*, 2006, **441**, 727–730.
24 F. Q. Potiguar and Y. Ding, *Phys. Rev. E*, 2013, **88**, 012204.
25 F. Tapia, D. Espíndola, E. Hamm and F. Melo, *Phys. Rev. E*, 2013, **87**, 014201.
26 B. Darbois-Texier and A. Seguin, *Phys. Rev. E*, 2022, **106**, 014906.
27 Y. Ding, N. Gravish and D. I. Goldman, *Phys. Rev. Lett.*, 2011, **106**, 028001.
28 F. Guillard, Y. Forterre and O. Pouliquen, *Phys. Fluids*, 2014, **26**, 043301.
29 S. Agarwal, A. Karsai, D. I. Goldman and K. Kamrin, *Science Advances*, 2021, **7**, eabe0631.
30 S. Agarwal, A. Karsai, D. I. Goldman and K. Kamrin, *Soft Matter*, 2021, **17**, 7196–7209.
31 S. Agarwal, D. I. Goldman and K. Kamrin, *Proc. Nat. Acad. Sci.*, 2023, **120**, e2214017120.
32 T. Lunne, J. J. Powell and P. K. Robertson, *Cone penetration testing in geotechnical practice*, CRC Press, 2002.
33 P. K. Robertson, *Can. Geotech. J.*, 2009, **46**, 1337–1355.
34 T. A. Brzinski III, P. Mayor and D. J. Durian, *Phys. Rev. Lett.*, 2013, **111**, 168002.
35 G. Meyerhof, *Geotechnique*, 1951, **2**, 301–332.
36 O. Pouliquen, *Physics of fluids*, 1999, **11**, 542–548.
37 K. Kamrin and G. Koval, *Phys. Rev. Lett.*, 2012, **108**, 178301.
38 M. Bouzid, M. Trulsson, P. Claudin, E. Clément and B. Andreotti, *Phys. Rev. Lett.*, 2013, **111**, 238301.
39 M. Bouzid, A. Izzet, M. Trulsson, E. Clément, P. Claudin and B. Andreotti, *Eur. Phys. J. E*, 2015, **38**, 125.
40 M. D. Bolton, M.-W. Gui, J. Garnier, J. F. Corte, G. Bagge, J. Laue and R. Renzi, *Géotechnique*, 1999, **49**, 543–552.
41 F. Patino-Ramirez and C. O'Sullivan, *Acta Geotech.*, 2023, **18**, 1–20.
42 W. S. Cleveland, *J. Am. Stat. Ass.*, 1979, **74**, 829–836.
43 F. Pacheco-Vázquez and J. Ruiz-Suárez, *Nature Comm.*, 2010, **1**, 123.
44 R. L. De La Cruz and G. Caballero-Robledo, *J. Fluid Mech.*, 2016, **800**, 248–263.
45 S. Pravin, B. Chang, E. Han, L. London, D. I. Goldman, H. M. Jaeger and S. T. Hsieh, *Phys. Rev. E*, 2021, **104**, 024902.
46 B. Chang and A. Kudrolli, *Phys. Rev. E*, 2022, **105**, 034901.